Korean J. Chem. Eng., 39(11), 3032-3038 (2022)
DOI: 10.1007/s11814-022-1194-0

pISSN: 0256-1115
eISSN: 1975-7220

Characterization and performance of $Sm_xA_{1-x}MnO_3$ (A=Ce, Sr, Ca) perovskite for efficient catalytic oxidation of toluene

Jing Hu*, Jiabin Zhou*,†, Tianlei Zhang*, Su Liu*, and Ke Du,†**

*School of Chemistry and Chemical Engineering, Southwest Petroleum University, Chengdu 610500, China
**Department of Mechanical and Manufacturing Engineering, University of Calgary, Calgary, Alberta, T2N 1N4, Canada
(*Received 14 December 2021 • Revised 22 May 2022 • Accepted 30 May 2022*)

Abstract−Catalytic oxidation of toluene was implemented over $SmMnO_3$, $Sm_{0.8}A_{0.2}MnO_3$ (ABO_3, A=Ce, Sr, Ca) and $Sm_{1-x}Ca_xMnO_3$ (x=0.0, 0.1, 0.2, 0.3) perovskite oxides synthesized via sol-gel method. The effects of A-site substitution of $SmMnO_3$ and the amount of calcium substitution of $SmMnO_3$ perovskite-type catalyst on the catalytic activity of toluene were investigated in a fixed bed reactor. The structure and chemical properties of the perovskites were studied by XRD, SEM, XPS, and H_2-TPR. The results showed that the substitution of Ce and Ca had a positive impact about the catalytic properties of toluene oxidation, while a negative impact was caused by the substitution of Sr. The catalytic activity of toluene oxidation followed the order of $Sm_{0.8}Ca_{0.2}MnO_3$>$Sm_{0.8}Ce_{0.2}MnO_3$>$SmMnO_3$>$Sm_{0.8}Sr_{0.2}MnO_3$ in terms of the temperature of $T_{90\%}$, at toluene concentration=1,000 ppm and weight hourly space velocity (WHSV)=3,000 mL/g·h. $Sm_{0.8}Ca_{0.2}MnO_3$ had the highest catalytic capacity ($T_{90\%}$=238 °C), which could be attributed to its high adsorbed oxygen concentration, Mn^{4+}/Mn^{3+}, and the best low-temperature reducibility (H_2 consumption=0.36). Meanwhile, the $Sm_{0.8}Ca_{0.2}MnO_3$ catalysts showed great long-term stability after 30 h of the reaction, and the toluene degradation rate remained over 95% at 350 °C.

Keywords: Perovskite Catalyst, A-site Substitution, Catalytic Oxidation, $SmMnO_3$, Adsorbed Oxygen

INTRODUCTION

Volatile organic compounds (VOCs) are significant precursors for the generation of ozone and secondary organic aerosols [1], which could have a negative effect on human health and the ecological environment [2,3]. Common VOC control technologies include condensation [4], absorption [5], adsorption [6], low-temperature plasma [7], photocatalysis [8], and catalytic oxidation [6,9]. Among these treatment technologies, catalytic oxidation technology has the advantages of low energy consumption, high efficiency, no secondary pollution, and the ability to convert organic matter into carbon dioxide and water. It has become one of the most promising VOC treatment technologies [10]. The efficiency of catalytic oxidation technology mainly depends on the catalyst material. At present, the commonly studied catalysts include noble metal (Au, Pd, Pt, Rh, Ru, etc.) [11,12], transition metal oxides (Cu, Fe, Mn, Co, etc.) [12] and composite metal oxide catalysts. Noble metal catalysts show great performance in the process of VOCs oxidation. These catalysts all have good catalytic activity, low reaction temperature, and great stability. However, they have the defects of high cost, easy to sinter at high temperature, carbon deposits, and its ability to resist sulfur poisoning is poor [13]. The use of transition metal oxides in VOCs catalytic oxidation technology has attracted extensive attention because of their low price, high stability, good anti-poisoning ability and rich surface oxygen vacancies [14].

Recently, the composite metal oxide catalysts formed by a variety of transition metals have been intensively studied due to their better redox ability than a single metal oxide [15]. Perovskite oxide (ABO_3), a composite metal oxide catalyst, has the advantages of low cost, controllable chemical composition, high stability, rich surface oxygen vacancies, and flexible oxygen mobility [16]. In perovskite oxide structure, A-site ions are composed of rare earth metal elements or alkaline earth metal elements with large radius, such as La, Ce. B-site ions are composed of transition metal elements with small radius, such as Mn, Co, Fe [17]. Among them, the element at position A mainly stabilizes the perovskite structure and affects the valence state, while the element at position B determines the effect of the catalyst. Zhang et al. [18] have prepared perovskite $LaMnO_3$ catalysts using citric acid sol-gel method, and co-precipitation method, respectively. The catalytic performance investigation shows that the catalysts prepared with different methods can completely convert p-toluene to CO_2 below 350 °C, which confirms that perovskite oxide has good catalytic oxidation performance.

Rare-earth element Sm has attracted wide attention recently because of its good vehicle exhaust purification and VOCs matter removal properties. Meanwhile, it is worth noting that Sm has strong oxygen storage ability and can increase oxygen absorption capture by catalysts [14,19-21]. Transition metal Mn has high catalytic activity, and manganese ore resources are abundant. Herein, we prepared $SmMnO_3$ perovskite-type oxides using the sol-gel method. Furthermore, for perovskite oxides, redox capacity and oxygen defects can be modified by partially replacing other cations with similar oxidation states and similar ionic radii in the A-site or B-site. The effects of Ce, Sr and Ca substitution sites on the oxidation of tolu-

†To whom correspondence should be addressed.
E-mail: jbzhou@swpu.edu.cn, kddu@ucalgary.ca

ene over $SmMnO_3$ catalyst were studied. The microstructure and chemical properties of the perovskites were analyzed with XRD, SEM, XPS, and H_2-TPR.

EXPERIMENTAL

1. Catalyst Preparation

The $SmMnO_3$, substituted $Sm_{0.8}A_{0.2}MnO_3$ (A=Ce, Sr and Ca) and $Sm_{1-x}Ca_xMnO_3$ (x=0.0, 0.1, 0.2, 0.3) perovskite oxide materials were prepared using the sol-gel method, as were the pure $SmMnO_3$ perovskite oxides too, which requires the temperature be controlled between 700 and 800 °C [22]. Therefore, we selected the preparation temperature of 800 °C to prepare $SmMnO_3$ and $Sm_{0.8}A_{0.2}MnO_3$ (A=Ce, Sr, and Ca). $Mn(NO_3)_2{\cdot}4H_2O$, $Sm(NO_3)_3{\cdot}6H_2O$, $Ce(NO_3)_2{\cdot}6H_2O$, $Sr(NO_3)_2$, and $Ca(NO_3)_2{\cdot}4H_2O$ with appropriate ratios were dissolved in deionized water. Then the solution was heated magnetically in a 90 °C water bath and citric acid was added to the solution. The molar ratio of citric acid to the metal cations was fixed at unity. Subsequently, the mixed solution was evaporated at 90 °C until the gel engendered. In order to carry out the gel decomposition, this wet gel was transferred to an oven and stored overnight for 12 h at 120 °C. Then, the obtained dry gel was calcined at 800 °C (2 °C/min) temperature for 2 h.

2. Catalyst Characterization

The crystal structure of the catalyst surface was analyzed by D8 Advance single-crystal X-ray diffractometer (XRD) of Brooke Company in the United States using Cu Kα irradiation. The X-ray tube was operated at 40 kV and the powder diffraction patterns were recorded in steps of 0.02° for 2θ between 10° and 80°. The morphology of the particles and distribution of chemical elements in the samples was characterized by a JEM-7500F emission scanning electron microscope (SEM). The catalyst's chemical composition and elemental valence were analyzed by ESCALAB 250 Xi X-ray photoelectron spectroscopy (XPS). The DAS-7000 high-performance dynamic adsorption instrument of Hunan Huasi Instrument Co, Ltd was used for H_2-TPR characterization. 50 mg of the catalyst was pretreated with N_2 at 300 °C for 1 h and cooled to room temperature. Then, the catalyst was exposed to 5% H_2/N_2 stream and raised to 900 °C at 10 °C/min to obtain the curve of H_2 consumption changing with temperature.

3. Catalyst Activity Evaluation

A fixed bed reactor was used for the catalytic oxidation of toluene and the performance evaluation of the catalyst. 0.2 g catalyst with particle size of 40-60 mesh is filled into the quartz reaction tube with inner diameter of 6 mm. The catalyst was placed in the middle of the quartz tube and both ends were plugged with quartz cotton to prevent catalyst leaking. A thermocouple was inserted into the lower end of the quartz reaction tube to monitor the temperature in the reaction process. The air was used as the carrier gas. After passing through the toluene generator, the air was mixed with the toluene gas. The flow of the toluene generator was adjusted to control the generation of 1,000 ppm toluene mixture. After passing through the gas flow controller, the mixture entered the fixed bed reactor at a flow rate of 100 ml/min. To investigate the catalytic activity of the catalyst for toluene at different temperatures, the reaction time at each temperature was at least 40 min. The FID detector of Shimadzu GC-2014C gas chromatograph was used to determine the mass concentration of toluene at the import and export of the reactor. The catalyst activity is expressed by the toluene conversion rate η, and it is calculated according to the following formula:

$$\eta_{toluene} = \frac{C_o - C}{C_o} \times 100\%$$

where C_o and C are the toluene concentration in the influent and effluent gas streams, respectively.

RESULTS AND DISCUSSION

1. Structural Properties

Fig. 1 shows the XRD patterns of $SmMnO_3$ and $Sm_{0.8}A_{0.2}MnO_3$, respectively. The XRD patterns of the catalysts show typical diffraction peaks of rhombic $SmMnO_3$ (JCPDS 25-0747), and the characteristic peaks at 2θ are 32.96°, 33.42°, 41.40°, 48.62°, 59.56°, and 69.17°, corresponding to (112), (200), (202), (004), (312) and (042) crystal surfaces, respectively. After partial substitution of samarium, the crystal structure of $SmMnO_3$ remained unchanged [23]. No diffraction peaks for Sm_2O_3 and MnO_x species were discovered in all the samples because of the detection limit of the X-ray diffractometer. When Sm^{2+} was replaced by Ce^{4+}, Sr^{2+}, and Ca^{2+}, the main characteristic peak shifted slightly at 32.96°, which may be due to the difference between the ionic radius of Sm^{2+} and the ionic radicals of Ce^{4+}, Sr^{2+} and Ca^{2+} [24]. This result is because the doped metals have been doped into the perovskite lattice. The ions between Sm^{2+} and the doped metal can alter the lattice volume due to free radical differences, thus constituting a defect in the perovskite structure [25]. The XRD patterns of all catalyst samples calcined at 800 °C show that the perovskite diffraction peak is sharp and clear, indicating that perovskite has been formed. With the doping of calcium, the XRD peak intensity of the catalyst gradually increases, indicating that the perovskite catalyst has small grains and many lattice defects. Such grains and lattice defects cause the perovskite

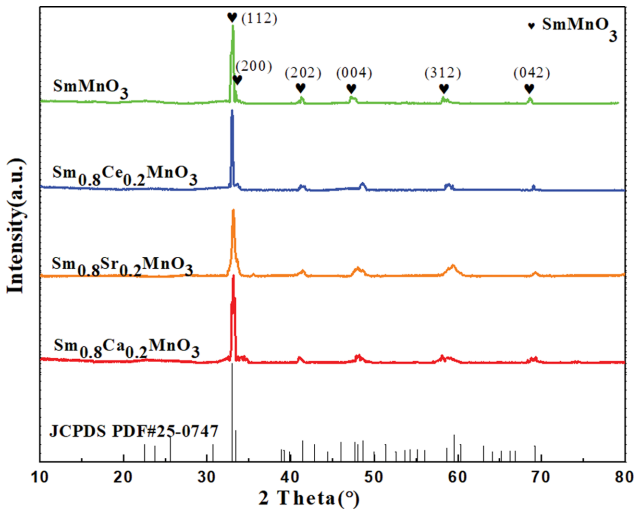

Fig. 1. XRD patterns of $SmMnO_3$ and $Sm_{0.8}A_{0.2}MnO_3$ (B=Ce, Sr, and Ca) catalysts.

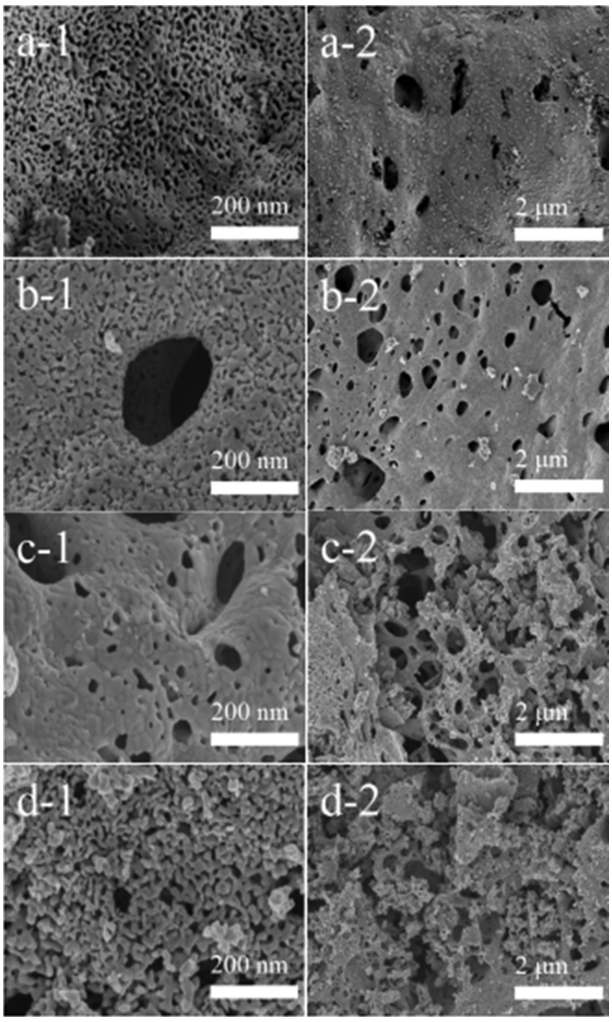

Fig. 2. SEM images of the catalysts: (a) $SmMnO_3$, (b) $Sm_{0.8}Ce_{0.2}MnO_3$, (c) $Sm_{0.8}Sr_{0.2}MnO_3$, (d) $Sm_{0.8}Ca_{0.2}MnO_3$.

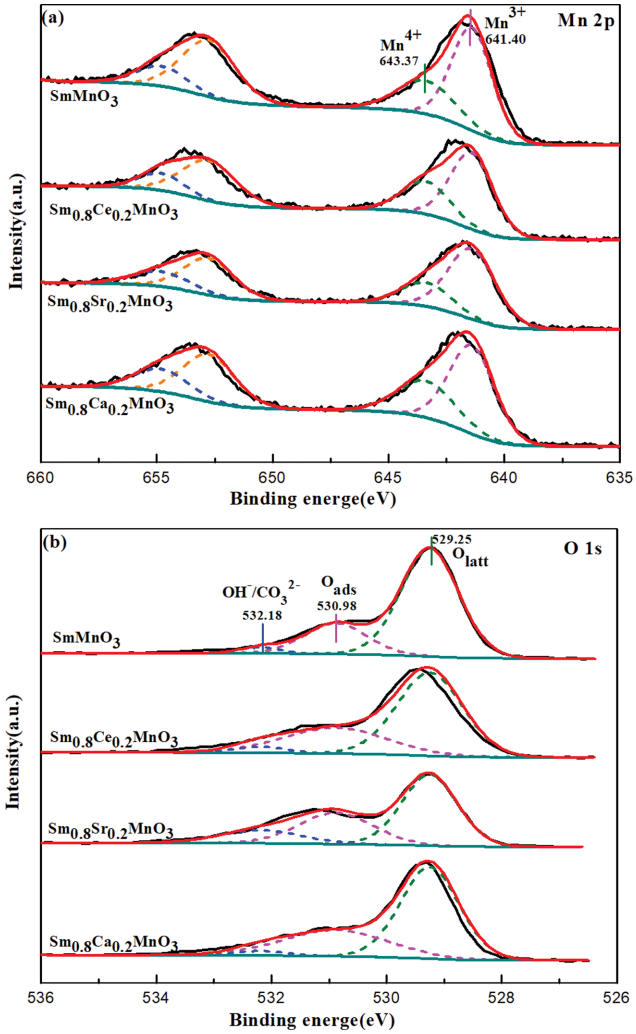

Fig. 3. XPS spectra of $SmMnO_3$ and $Sm_{0.8}A_{0.2}MnO_3$ (A=Ce, Sr and Ca) catalysts.

catalyst to be more conducive and thereby improve its catalytic oxidation performance [26].

2. Morphology Characteristics

The morphology and particle size of $SmMnO_3$ and $Sm_{0.8}A_{0.2}MnO_3$ (A=Ce, Sr, and Ca) perovskites were studied using scanning electron microscopy. Fig. 2 is an SEM photograph of perovskite type oxides. As can be seen from the SEM photographs in Fig. 2a-2, b-2, c-2, and d-2, all samples have obvious pores. When enlarged, Fig. 2a-1 shows that $SmMnO_3$ catalyzer presents an ordered continuous porous network structure. From the photographs in Fig. 2c-1, we can see that the substances on the surface of the $Sm_{0.8}Sr_{0.2}MnO_3$ catalyst sample coagulated into blocks, which proves that crystal growth and particle agglomeration lead to increased crystallinity with the doping of strontium into $SmMnO_3$ [27]. However, it can be observed from Fig. 2d-1 that the surface of the Ca-substituted oxide contains a very rich honeycomb-like pore structure, which can increase the contact area of the catalyst and the reactant and facilitate the progress of the catalytic reaction. At the same time, from Fig. 2d-1, the pores of $Sm_{0.8}Ca_{0.2}MnO_3$ catalyst increase and the aperture becomes larger. This structure is conducive to the entry of toluene into the inner surface of the catalyst and affects the residence time of toluene in the pores. This catalyst reacts more fully with toluene.

3. XPS Analysis

The chemical composition, chemical valence, and metal oxidation state of pure $SmMnO_3$ and $Sm_{0.8}A_{0.2}MnO_3$ (A=Ce, Sr and Ca) catalysts were analyzed using XPS. Fig. 3 shows the recorded Mn2p and O1s XPS spectrum of perovskites. Fig. 3(a) shows the XPS spectra of sample Mn2p. There is an asymmetric Mn2p peak at 642.01 ev. This spectral curve can be divided into two peaks, Mn^{3+} of 641.40 ev and Mn^{4+} of 643.37 ev, respectively. The higher Mn^{4+}/Mn^{3+} molar ratio indicates that the catalyst has stronger redox ability. As shown in Table 1, the Ca substituted sample shows the highest Mn^{4+} concentration, and the Sr substituted samples has lower Mn^{4+} concentration. With the partial substitution of calcium for $SmMnO_3$ catalyst, the molar ratio of Mn^{4+}/Mn^{3+} increases from 0.46 to 0.53; this is coincident with the activity results of the catalyst for catalytic oxidation of toluene in Fig. 5, a significantly increased surface Mn^{4+} concentration of the $SmMnO_3$ catalyst was indicated. According to the principle of electric neutrality, ABO_3

Table 1. Composition of catalyst surface elements

Samples	Mn^{4+}/Mn^{3+}	O_{ads}/O
$SmMnO_3$	0.46	0.31
$Sm_{0.8}Ce_{0.2}MnO_3$	0.48	0.49
$Sm_{0.8}Sr_{0.2}MnO_3$	0.35	0.27
$Sm_{0.8}Ca_{0.2}MnO_3$	0.53	0.52

Table 2. H_2-uptakes of $SmMnO_3$ and $Sm_{0.8}A_{0.2}MnO_3$ (A=Ce, Sr, and Ca) catalysts (mmol·g^{-1})

Samples	T<275 °C	275 °C<T<450 °C	T>450 °C	Total
$SmMnO_3$	0.17	0.40	1.99	2.56
$Sm_{0.8}Ce_{0.2}MnO_3$	0.35	1.40	1.13	2.88
$Sm_{0.8}Sr_{0.2}MnO_3$	0.03	1.26	1.01	2.30
$Sm_{0.8}Ca_{0.2}MnO_3$	0.36	1.21	1.71	3.28

has three components: $A^{1+}B^{5+}O_3$, $A^{2+}B^{4+}O_3$, and $A^{3+}B^{3+}O_3$. The doping of Ca^{2+} leads to the increase of Mn^{4+} content in $SmMnO_3$ perovskite oxide, doping Ca increase Mn's mass fraction as Sm has a larger molecular weight than Ca. In $Sm_{0.8}Ca_{0.2}MnO_3$ perovskite oxide, Mn^{4+} has good oxygen mobility and strong oxidizing ability to reduce to Mn^{3+}. Fig. 3(b) is the XPS spectrum of all the sample O1s. As can be seen from Fig. 3(b), there are a variety of oxygen species on the surface of the four perovskites, including lattice oxygen at 529.25 ev (e.g., O^{2-}), adsorbed oxygen at 530.98 ev (e.g., O_2^-, O_2^{2-}) and carbonate or hydroxyl at 532.18 ev [28]. Table 1 shows the calculated O_{ads}/O molar ratio in the $Sm_{0.8}Ca_{0.2}MnO_3$ sample was the highest, followed by $Sm_{0.8}Ce_{0.2}MnO_3$. However, the O_{ads}/O ratio in the $Sm_{0.8}Sr_{0.2}MnO_3$ samples was lower than the $SmMnO_3$ sample. As far as O_{ads}/O molar ratio, the ordering was consistent with the catalysts reducibility in the H_2-TPR. The O_{ads}/O molar ratio order for the four samples is $Sm_{0.8}Ca_{0.2}MnO_3$>$Sm_{0.8}Ce_{0.2}MnO_3$>$SmMnO_3$>$Sm_{0.8}Sr_{0.2}MnO_3$, which suggests that the $Sm_{0.8}Ca_{0.2}MnO_3$ oxide can provide the most adsorbed oxygen.

4. Reducibility

Fig. 4 shows the TPR peak spectra of A-site substitution by Ce, Sr, and Ca for $SmMnO_3$ perovskites catalysts. As shown, there are two reduction peaks in the catalysts. The reduction peak below 450 °C can be considered as reducing Mn^{3+} to Mn^{2+} on the surface, and the reduction peaks at 683 °C, 545 °C, 617 °C and 584 °C can be considered as the reduction of the remaining Mn^{3+} to Mn^{2+} in deeper region of the catalysts [15,23,29]. Table 2 summarizes the H_2 consumption of different temperature ranges by analyzing the area of reduction peaks in the H_2-TPR spectrum. For these four catalysts, we found two main reduction peaks. The two reduction peaks are in the low temperature range of 100-450 °C and the high temperature range of 450-800 °C respectively.

In the low-temperature range, the H_2 consumption of $SmMnO_3$, $Sm_{0.8}Ce_{0.2}MnO_3$, $Sm_{0.8}Sr_{0.2}MnO_3$, and $Sm_{0.8}Ca_{0.2}MnO_3$ perovskites below 275 °C was 0.17, 0.35, 0.03, and 0.36 mmol·g^{-1}, respectively. The highest H_2 consumption of $Sm_{0.8}Ca_{0.2}MnO_3$ can be attributed to the high oxygen adsorption content on its surface. Moreover, the substitution of Ce and Ca can promote the original $SmMnO_3$ reducibility [30]. The presence of doped metals influences the reducibility of the A-site substituted perovskites. The reduction peaks of $Sm_{0.8}Ca_{0.2}MnO_3$ and $Sm_{0.8}Ce_{0.2}MnO_3$ samples are at 228 °C and 330 °C. In the catalytic activity evaluation reaction, the test activity temperature is lower than 350 °C. As can be seen from Fig. 5, when the temperature is lower than 275 °C, the catalytic oxidation of toluene by all catalysts is about 90%. Therefore, Table 2 shows that when the temperature is lower than 275 °C, the order of hydrogen consumption of the four catalysts is: $Sm_{0.8}Ca_{0.2}MnO_3$>$Sm_{0.8}Ce_{0.2}MnO_3$>$SmMnO_3$>$Sm_{0.8}Sr_{0.2}MnO_3$. $Sm_{0.8}Ca_{0.2}MnO_3$ has the largest hydrogen consumption of 0.36 mmol·g^{-1}. It shows that $Sm_{0.8}Ca_{0.2}MnO_3$ has many kinds of surface active oxygen and stronger catalytic oxidizing ability. In the temperature range of 275 °C-450 °C, two partially overlapping peaks occurred. During this period, the H_2 consumption of $SmMnO_3$, $Sm_{0.8}Ce_{0.2}MnO_3$, $Sm_{0.8}Sr_{0.2}MnO_3$ and $Sm_{0.8}Ca_{0.2}MnO_3$ samples was 0.40, 1.40, 1.26, and 1.21 mmol·g^{-1}, respectively. These phenomena suggest that partial substitution of

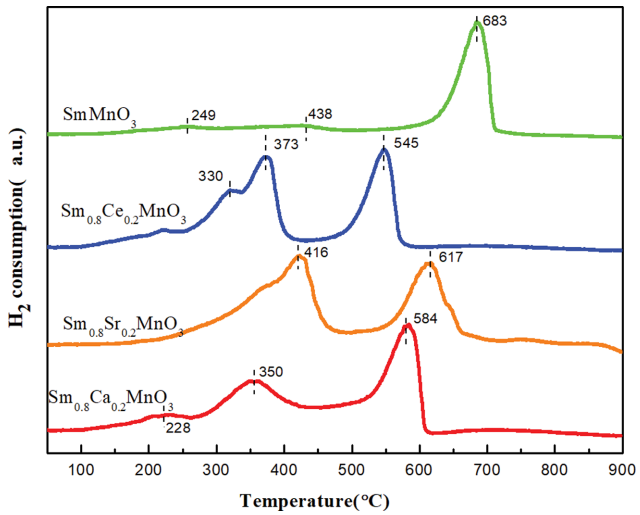

Fig. 4. H_2-TPR profiles of $SmMnO_3$ and $Sm_{0.8}A_{0.2}MnO_3$ (A=Ce, Sr, and Ca) catalysts.

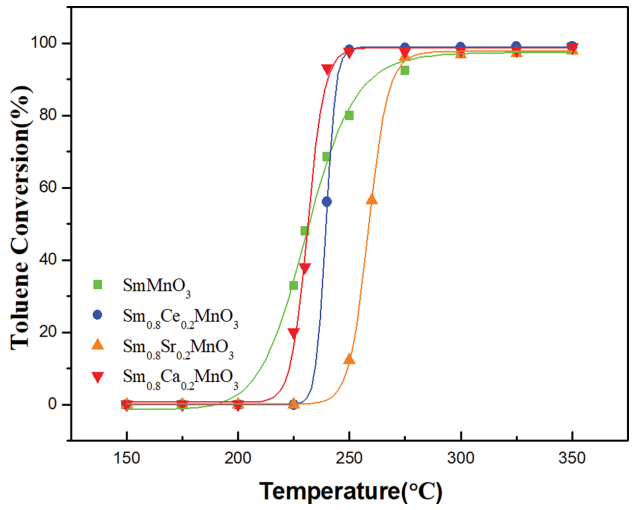

Fig. 5. Catalytic activity of $SmMnO_3$ and $Sm_{0.8}A_{0.2}MnO_3$ (A=Ce, Sr and Ca) for toluene.

Table 3. Reaction temperatures for 50% and 90% toluene conversion

Catalyst	$T_{50\%}$/°C	$T_{90\%}$/°C
$SmMnO_3$	230	263
$Sm_{0.8}Ce_{0.2}MnO_3$	239	246
$Sm_{0.8}Sr_{0.2}MnO_3$	256	276
$Sm_{0.8}Ca_{0.2}MnO_3$	230	238

Ca and Ce for perovskite metal cations enhances the catalytic performance of $SmMnO_3$, whereas partial substitution of Sr has negative influence on the catalytic performance.

When the reaction temperature was 450 °C to 850 °C, the H_2 consumption of $SmMnO_3$, $Sm_{0.8}Ce_{0.2}MnO_3$, $Sm_{0.8}Sr_{0.2}MnO_3$ and $Sm_{0.8}Ca_{0.2}MnO_3$ samples was 1.99, 1.13, 1.01, and 1.71 mmol·g^{-1}, respectively. The high consumption of H_2 during this high temperature is because the Mn^{3+} is partially reduced to Mn^{2+} [30].

5. Catalytic Activity Tests

When WHSV=30,000 mL/g·h and initial toluene concentration was 1,000 ppm, we carried out a series of tests on the toluene-catalyzed oxidation reaction on the four perovskite catalysts. Fig. 5 indicates that the toluene degradation rates approached 100% for all catalysts at temperatures below 350 °C. Table 3 presents the representative parameters of $T_{50\%}$ and $T_{90\%}$, which represent the temperature for toluene conversion rate at 50% and 90%. The Ca-substituted of $SmMnO_3$ had the best catalytic activity. When the amount of Ca substitution was 0.2, the $T_{50\%}$ of the samples was almost identical to the $SmMnO_3$, which was 230 °C. But the $T_{90\%}$ of $Sm_{0.8}Ca_{0.2}MnO_3$ was 238 °C, which is 25 °C lower than the pure sample $SmMnO_3$. Secondly, the $T_{50\%}$ and $T_{90\%}$ of $Sm_{0.8}Ce_{0.2}MnO_3$ were 239 °C and 246 °C, respectively. In the high-temperature reaction stage, $Sm_{0.8}Ce_{0.2}MnO_3$ and $Sm_{0.8}Ca_{0.2}MnO_3$ had a certain promoting effect on the oxidation of toluene when compared with $SmMnO_3$. However, the $T_{50\%}$ and $T_{90\%}$ of $Sm_{0.8}Sr_{0.2}MnO_3$ were 256 °C and 276 °C, respectively; it is shown that the partial substitution of Sr negatively affects the catalytic properties of $SmMnO_3$. In terms of the conversion rate, $Sm_{0.8}Sr_{0.2}MnO_3$ was considered the worst effective catalyst in toluene oxidation in this study. $Sm_{0.8}Ca_{0.2}MnO_3$ shows lower $T_{90\%}$ than $Sm_{0.8}Ce_{0.2}MnO_3$, which indicates that $Sm_{0.8}Ca_{0.2}MnO_3$ has better low-temperature activity. The catalytic activity of Ca-substituted $SmMnO_3$ with other reported perovskite oxides is summarized in Table 4 [31-34]. For convenience, $T_{50\%}$ and $T_{90\%}$ were chosen to compare the catalytic performance of catalysts reported and synthesized in this work. For sample $Sm_{0.8}Ca_{0.2}MnO_3$, it shows better performance when compared with other reported samples.

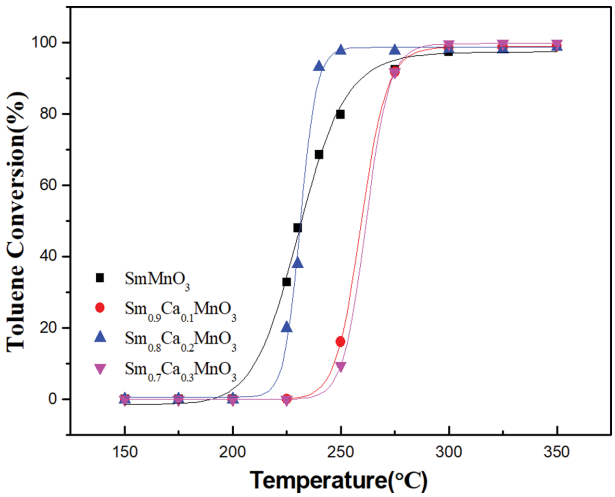

Fig. 6. Catalytic activity of $Sm_{1-x}Ca_xMnO_3$ (x=0, 0.1, 0.2, 0.3) for toluene.

It can be seen that Ca-substituted of $SmMnO_3$ samples exhibit superior performance for toluene catalytic oxidation than reported catalysts. Therefore, the catalyst with Ca-substituted at 0.2 of $SmMnO_3$ can greatly improve its catalytic performance for toluene oxidation.

Based on the influence of Ce, Sr, and Ca substitution of A-sites on the catalytic properties for toluene oxidation of $SmMnO_3$ (Fig. 5), it can be seen that calcium substitution at 0.2 has the best catalytic oxidation effect on toluene. The calcium substitution can increase the surface area and pore volume of the catalysts [35]. Therefore, how the amount of calcium substitution influences the catalytic toluene oxide properties of $SmMnO_3$ perovskite-type catalyst is further discussed. Fig. 6 shows the catalytic oxidation curve of $Sm_{1-x}Ca_xMnO_3$ (x=0.0, 0.1, 0.2, 0.3) perovskite catalyst for toluene. In the case of calcium substitution at 0.2, the $T_{90\%}$ of $Sm_{0.8}Ca_{0.2}MnO_3$ was 238 °C, which was 25 °C lower than the pure sample $SmMnO_3$, showing that calcium substitution at 0.2 promoted the catalytic oxidation of toluene. When the substitution of calcium was 0.1 and 0.3, the temperature of $T_{50\%}$ and $T_{90\%}$ showed an increased trend; the $T_{50\%}$ and $T_{90\%}$ of $Sm_{0.9}Ca_{0.1}MnO_3$ were 262 °C and 273 °C, and the $T_{50\%}$ and $T_{90\%}$ of $Sm_{0.7}Ca_{0.3}MnO_3$ were 263 °C and 274 °C. By comprehensive consideration of the conversion process and the two representative parameters of $T_{50\%}$ and $T_{90\%}$, the sample of $Sm_{0.7}Ca_{0.3}MnO_3$ was considered the worst active catalyst among the four samples of $Sm_{1-x}Ca_xMnO_3$ (x=0.0, 0.1, 0.2, 0.3). The appropriate amount of Ca substitution in $SmMnO_3$ perovskite enhanced the Mn^{4+}/Mn^{3+} ratio and oxygen density, which could improve the

Table 4. Comparison of the catalytic activity of Ca-substituted $SmMnO_3$ with other reported perovskite oxides

Catalyst	Preparation method	Catalytic activity ($T_{50\%}$)	Catalytic activity ($T_{90\%}$)	Reference
$GdMnO_3$ (SY)-0.05	Sol-gel	234	256	Guo et al. [31]
$LaMnO_3/\delta$-MnO_2	Gunpowder-like combustion method	248	258	Yang et al. [32]
$LaMnO_3/TiO_2$	Sol-gel	278	303	Giroir-Fendler et al. [33]
$SrTi_{1-x}Mn_xO_3$	One-pot hydrothermal	302	335	Suarez-Vazquez et al. [34]
$Sm_{0.8}Ca_{0.2}MnO_3$	Sol-gel	230	238	This work

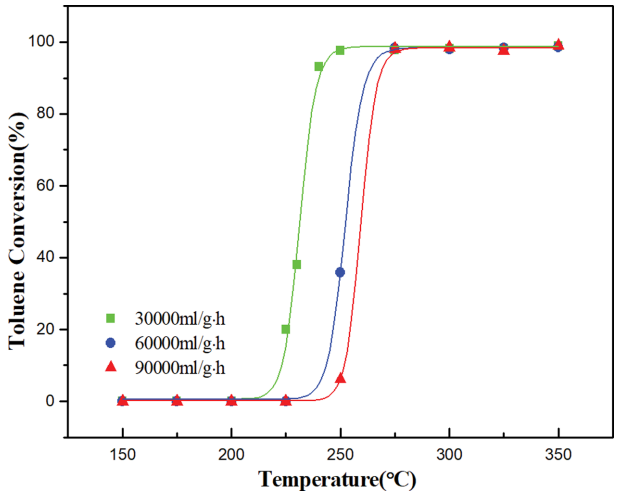

Fig. 7. Effect of WHSV on catalytic oxidation of toluene.

catalytic performance. The substitution of Sm was able to produce an electronic imbalance of perovskite structure. But the catalytic activity did not increase with the amount of calcium substitution, indicating that calcium substitution of $SmMnO_3$ perovskite had multiple effects on toluene conversion.

To evaluate the unit treatment capacity of the catalytic device, the catalytic oxidation performance of $Sm_{0.8}Ca_{0.2}MnO_3$ perovskite oxide for toluene was evaluated in terms of weight hourly space velocity (WHSV). When the initial concentration of toluene was 1,000 ppm, the effect of $Sm_{0.8}Ca_{0.2}MnO_3$ catalyst on the catalytic oxidation of toluene at different space velocities is shown in Fig. 7. With the increase of WHSV, the degradation of toluene by $Sm_{0.8}Ca_{0.2}MnO_3$ decreased. For the Ca-substituted sample, the $T_{50\%}$ and $T_{90\%}$ values of toluene oxidation at WHSV=30,000 mL/g·h were 230 °C and 238 °C, which were 28 °C and 25 °C lower than that at WHSV=60,000 mL/g·h. When WHSV rose to 90,000 ml/g·h, the catalytic oxidation effect of toluene was the worst, $T_{50\%}$=261 °C, $T_{90\%}$=270 °C. The results show that the WHSV has a certain impact on the catalytic oxidation capacity of the catalyst, and the toluene oxidation efficiency will decrease with the increase of WHSV. The negative effect of WHSV on oxidation efficiency is due to the short residence time of toluene gas on the catalyst surface at higher flow rate.

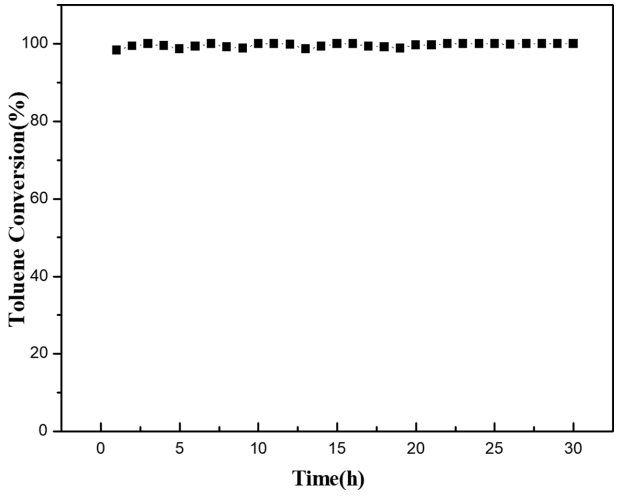

Fig. 8. Evaluation of reaction stability of $Sm_{0.8}Ca_{0.2}MnO_3$ catalyst.

The stability of the catalyst is an important indicator to evaluate the catalyst performance. The stability test of $Sm_{0.8}Ca_{0.2}MnO_3$ is shown in Fig. 8. As can be seen, when the reaction temperature is 350 °C, the WHSV of 30,000 mL/g·h, initial toluene concentration of 1,000 ppm, and continuous catalytic oxidation of toluene for 30 hours, almost complete conversion of toluene was observed, indicating that $Sm_{0.8}Ca_{0.2}MnO_3$ catalyst has relatively good activity and stability.

CONCLUSIONS

$SmMnO_3$, $Sm_{0.8}A_{0.2}MnO_3$ (A=Ce, Sr and Ca) and $Sm_{1-x}Ca_xMnO_3$ (x=0.0, 0.1, 0.2, 0.3) perovskite oxide materials were prepared by sol-gel method. The catalyst activity experiment confirmed that the substitution of Ce and Ca has a positive influence on the catalytic properties of toluene oxidation, while a negative effect was observed for the substitution of Sr. Under optimal conditions, $Sm_{0.8}Ca_{0.2}MnO_3$ had the best catalytic performance of toluene oxidation with $T_{90\%}$=238 °C, which was much lower than the pure sample $SmMnO_3$. The enhancement of catalytic activity could be ascribed to the increased adsorbed oxygen concentration and surface Mn^{4+}/Mn^{3+} ratio from the partial substitution of Ca on $SmMnO_3$. At WHSV=90,000 mL/g·h, $Sm_{0.8}Ca_{0.2}MnO_3$ catalyst still had good catalytic activity. Moreover, the 30 h oxidation test showed that $Sm_{0.8}Ca_{0.2}MnO_3$ catalyst has relatively good stability for continuous operation. This work could provide a facile route to prepare of ABO_3 perovskites with high catalytic activity at low temperature for VOCs removal.

ACKNOWLEDGEMENTS

This paper was supported by the Sichuan Science and Technology Program (2020YFS0305).

REFERENCES

1. M. S. Kamal, S. A. Razzak and M. M. Hossain, *Atmos. Environ.*, **140**, 117 (2016).
2. X. Li, Y. Niu, H. Su and Y. Qi, *Catal. Lett.*, **112**, 91 (2021).
3. C. A. Weitekamp, T. Stevens, M. J. Stewart, P. Bhave and M. I. Gilmour, *Sci. Total Environ.*, **04**, 135 (2020).
4. M. Song, K. Kim, C. Cho and D. Kim, *Processes*, **9**, 112 (2021).
5. P. F. Biard, A. Couvert and S. Giraudet, *J. Ind. Eng. Chem.*, **59**, 70 (2018).
6. C. Yang, G. Miao, Y. Pi, Q. Xia, J. Wu, Z. Li and J. Xiao, *Chem. Eng. J.*, **370**, 1128 (2019).
7. Z. Chang, C. Wang and G. Zhang, *Plasma Processes Polym.*, **17**, 332 (2020).
8. T. M. Fujimoto, M. Ponczek, U. L. Rochetto, R. Landers and E. Tomaz, *Environ. Sci. Pollut. Res. Int.*, **24**, 6390 (2017).
9. Y. Guo, M. Wen, G. Li and T. An, *Appl. Catal., B.*, **281**, 1336 (2021).

10. C. H. Zhang, C. Wang, S. Gil, A. Boreave, L. Retailleau, Y. L. Guo, J. L. Valverde and A. Giroir-Fendler, *Appl. Catal., B.*, **201**, 552 (2017).
11. G. Spezzati, A. D. Benavidez, A. T. DeLaRiva, Y. Su, J. P. Hofmann, S. Asahina, E. J. Olivier, J. H. Neethling, J. T. Miller, A. K. Datye and E. J. M. Hensen, *Appl. Catal. B*, **243**, 36 (2019).
12. X.-H. Yan, H.-F. Zhang, C.-L. Wu, C. Zhang and S.-H. Li, *Int. J. Inorg. Mater.*, **34**, 43 (2019).
13. H. Einaga, S. Hyodo and Y. eraoka, *Top. Catal.*, **53**, 629 (2010).
14. L. Liu, J. Sun, J. Ding, Y. Zhang, J. Jia and T. Sun, *Inorg. Chem.*, **58**, 14275 (2019).
15. P. Liu, G. Wei, X. Liang, D. Chen, H. He, T. Chen, Y. Xi, H. Chen, D. Han and J. Zhu, *Appl. Clay Sci.*, **161**, 265 (2018).
16. N. Rezlescu, E. Rezlescu, P. D. Popa, C. Doroftei and M. Ignat, *Composites, Part B*, **60**, 515 (2014).
17. S. Royer, D. Duprez, F. Can, X. Courtois, C. Batiot-Dupeyrat, S. Laassiri and H. Alamdari, *Chem. Rev.*, **114**, 10292 (2014).
18. C. Zhang, Y. Guo, Y. Guo, G. Lu, A. Boreave, L. Retailleau, A. Baylet and A. Giroir-Fendler, *Appl. Catal., B*, **148**, 490 (2014).
19. A. E. Hannora and F. F. Hanna, *J. Mater. Sci.: Mater. Electron.*, **30**, 12456 (2019).
20. L. Z. Liu, J. X. Li, H. B. Zhang, L. Li, P. Zhou, X. L. Meng, M. M. Guo, J. P. Jia and T. H. Sun, *J. Hazard. Mater.*, **362**, 178 (2019).
21. L. Z. Liu, H. B. Zhang, J. P. Jia, T. H. Sun and M. M. Sun, *Inorg. Chem.*, **57**, 8451 (2018).
22. J. Y. Min, L. L. Yu, P. S. Tang and H. F. Chen, *Key Eng. Mater.*, **748**, 403 (2017).
23. X. B. Zhu, X. Tu, M. H. Chen, Y. Yang, C. H. Zheng, J. S. Zhou and X. Gao, *Catal. Commun.*, **92**, 35 (2017).
24. X. Zhu, X. Gao, R. Qin, Y. Zeng, R. Qu, C. Zheng and X. Tu, *Appl. Catal. B*, **293**, 170 (2015).
25. J. Wang, Y. Su, X. Wang, J. Chen, Z. Zhao and M. Shen, *Catal. Commun.*, **25**, 106 (2012).
26. G. Fierro, M. Lo Jacono and M. Inversi, *Top. Catal.*, **10**, 39 (2000).
27. Y. Wu, L. Li, B. Chu, Y. Yi, Z. Qin, M. Fan, Q. Qin, H. He, L. Zhang, L. Dong, B. Li and L. Dong, *Appl. Catal. A*, **568**, 43 (2018).
28. N. Miniajluk, J. Trawczynski and M. Zawadzki, *Appl. Catal. A*, **531**, 119 (2017).
29. Y. Lu, Q. Dai and X. Wang, *Catal. Commun.*, **54**, 114 (2014).
30. C. Zhang, W. Hua, C. Wang, Y. Guo, Y. Guo, G. Lu, A. Baylet and A. Giroir-Fendler, *Appl. Catal. B*, **134**, 310 (2013).
31. M. Guo, L. Liu, J. Gu, H. Zhang, X. Min, J. Liang, J. Jia, K. Li and T. Sun, *Chin. J. Chem. Eng.*, **34**, 278 (2021).
32. J. Yang, L. Li, X. Yang, S. Song, J. Li, F. Jing and W. Chu, *Catal. Today*, **327**, 19 (2019).
33. A. Giroir-Fendler, M. lves-Fortunato, M. Richard, C. Wang, J. A. Diaz, S. Gil, C. Zhang, F. Can, N. Bion and Y. Guo, *Appl. Catal. B*, **180**, 29 (2016).
34. S. I. Suarez-Vazquez, S. Gil, J. M. Garcia-Vargas, A. Cruz-Lopez and A. Giroir-Fendler, *Appl. Catal. B*, **223**, 201 (2018).
35. X. Cui, H. Yang, J. Zhang, T. Wu, P. Zhao and Q. Guo, *Catal. Lett.*, **151**, 3323 (2021).